Quantitative and Qualitative Evaluation of a Three-Dimensional Mesoscale Numerical Model Simulation of a Sea Breeze in Complex Terrain

D. G. STEYN AND I. G. MCKENDRY*

Atmospheric Science Program, Department of Geography, The University of British Columbia, Vancouver, B.C., Canada

(Manuscript received 21 July 1987, in final form 9 March 1988)

ABSTRACT

This study presents an evaluation of the performance of the Colorado State University (CSU) three-dimensional numerical mesoscale model. The evaluation consists of quantitative and qualitative comparisons of the model output with observed data. The observations were undertaken in the lower Fraser Valley of British Columbia, Canada on 23 August 1985 utilizing up to 23 fixed stations for anemometry, three acoustic sounders, one tethersonde and one set of instruments for determining the surface energy budget terms.

The modeling covers a 24-hour period during which a well-developed sea breeze was observed. While the results of the model evaluation apply to the single case presented, they have implications for a wide range of cases. The statistical methods of Willmott are applied to hourly averaged variables to assess the model's performance.

The evaluation shows that the model is capable of providing very realistic wind and temperature fields within the broad coastal valley which makes up the bulk of the domain. The modeled mixed layer depth, surface energy budget terms and wind profiles are in good agreement with observed data.

1. Introduction

Much research effort over the past two decades has gone into the development of realistic numerical mesoscale meteorological models. Various models (or even families of models) have been developed using a range of numerical procedures for solving the prognostic equations, which have been derived from a variety of exact or parameterized representations of atmospheric processes. The variety of models extant in recent times has been ably summarized by Pielke (1984).

Development of mesoscale numerical models should proceed in response to a critical quantitative evaluation of the ability of existing models to reproduce observed atmospheric variability at temporal and spatial scales representative of the mesoscale. In order to maximize its discriminating power, the evaluation should be performed using as many of the model output variables as possible. It is the objective of this work to present just such a critical evaluation of one of the best-documented and most highly developed of the available mesoscale models using a wide range of measured variables. It is not the objective of this work to further model development or to discuss the details of the sea breeze as revealed by the model.

Previous quantitative evaluations of model performance (for example, Pielke and Mahrer 1978; Simpson et al. 1979; Segal et al. 1982) have been based on the work of Keyser and Anthes (1977) who defined a set of statistical measures for the comparison of model output with observations. They used the root-mean square difference (RMSD) between observed and modeled values. They also used the root-mean-square differences after correction (RMSDC) for the mean, and standard deviations of the two fields. Their quantitative evaluation was complemented by diagrams of the computed fields in plan view.

In reviews of methods for evaluating model performance (Willmott 1981, 1982; Willmott et al. 1985) Willmott recommends that quantitative evaluation of model performance be based upon the following parameters:

1. Observed and modeled means and standard deviations;
2. Systematic and unsystematic components of the root-mean-squared differences as well as the total root mean squared difference ($RMSD_s$, $RMSD_u$ and RMSD, respectively). These parameters are defined (Willmott 1982; Willmott et al. 1985) as:

$$RMSD_s = \left[\frac{1}{n}\sum_{1}^{n}(P_i^* - O_i)^2\right]^{1/2},$$

$$RMSD_u = \left[\frac{1}{n}\sum_{1}^{n}(P_i^* - P_i)^2\right]^{1/2},$$

* Present affiliation: New Zealand Meteorological Service, Wellington, New Zealand.

Corresponding author address: Dr. Douw G. Steyn, Dept. of Geography, 217-1984 West Mall, University of British Columbia, Vancouver, BC V6T 1W5.

and

$$\text{RMSD} = \left[\frac{1}{n}\sum^{n}(P_i - O_i)^2\right]^{1/2}.$$

Where n is the number of cases (evaluation points), P_i and O_i are predicted and observed values respectively and $P_i^* = a + bO_i$ where a and b are the parameters associated with an ordinary least-squares linear regression between O and P. If **P** and **O** are vectors, the difference measures must be calculated using the magnitudes of the vector differences and the P_i^* are vector components after Willmott et al. (1985)

3) The index of agreement d which is defined as

$$d = 1 - [n(\text{RMSD})^2/\sum_{1}^{n}(|P_i'| + |O_i'|)^2],$$

where $P_i' = P_i - \bar{O}$ and $O_i' = O_i - \bar{O}$, with $\bar{O}$ being the average observed value. This dimensionless index has a theoretical range of 1.0 (for perfect agreement) to 0.0 (for no agreement). Willmott (1981) questions the validity of reporting on the statistical significance of the above measures but argues that his set of measures includes that of Keyser and Anthes (1977) and carries more information than their more rudimentary set.

Before proceeding with the model evaluation it must be recognized that disagreement between observed and modeled results may arise from a number of sources, namely:

- Inadequacies in the model formulation. These may be due to the omission or only partial inclusion of processes of significance to the phenomenon being modelled, or may be due to inaccuracies inherent in the numerical implementation of the model equations.
- Disagreement that arises because of the finite tem-

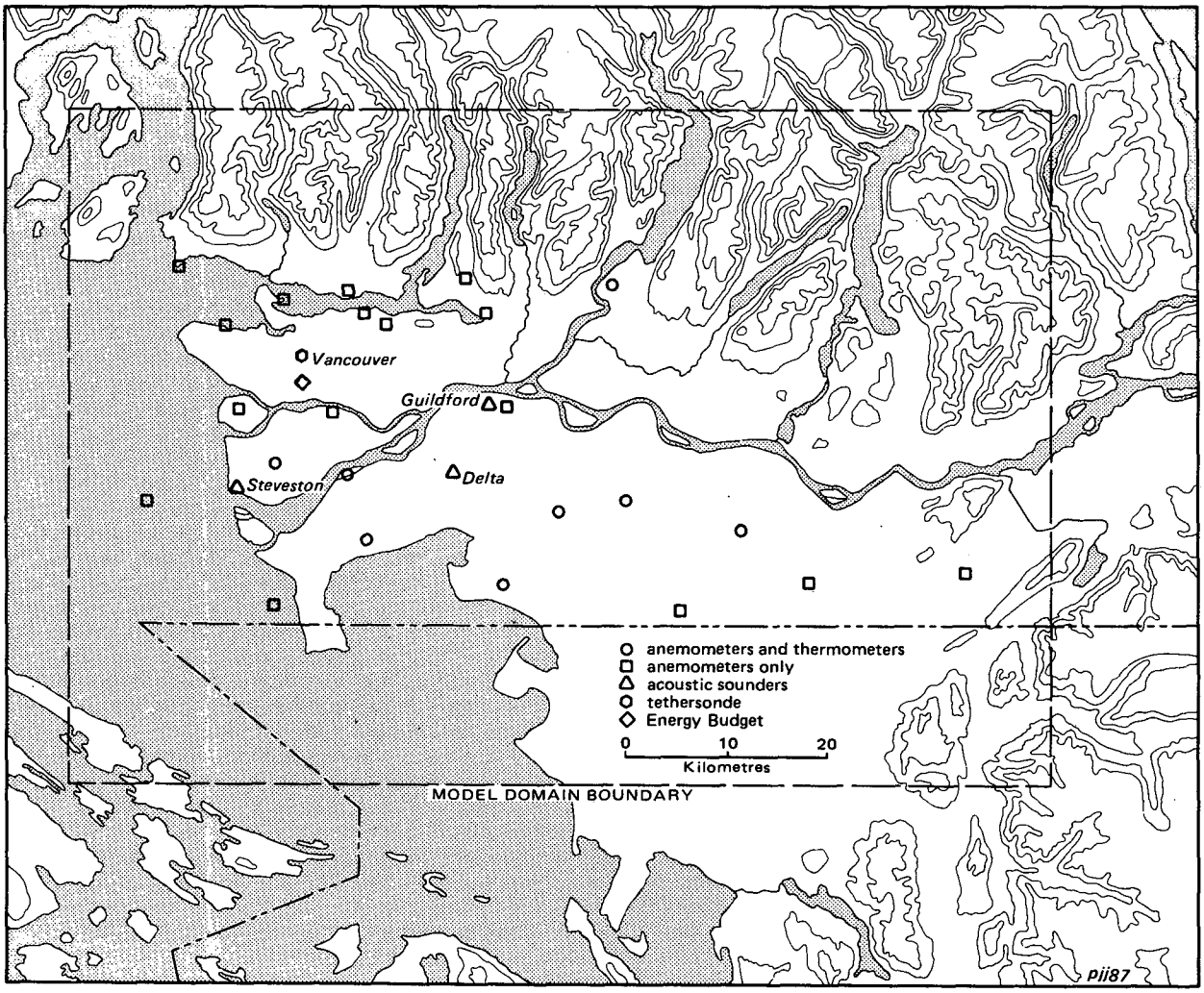

FIG. 1. Map of the modeling domain and surrounding topography, showing the location of the network of stations at which evaluation data were gathered. Contour interval is 300 m.

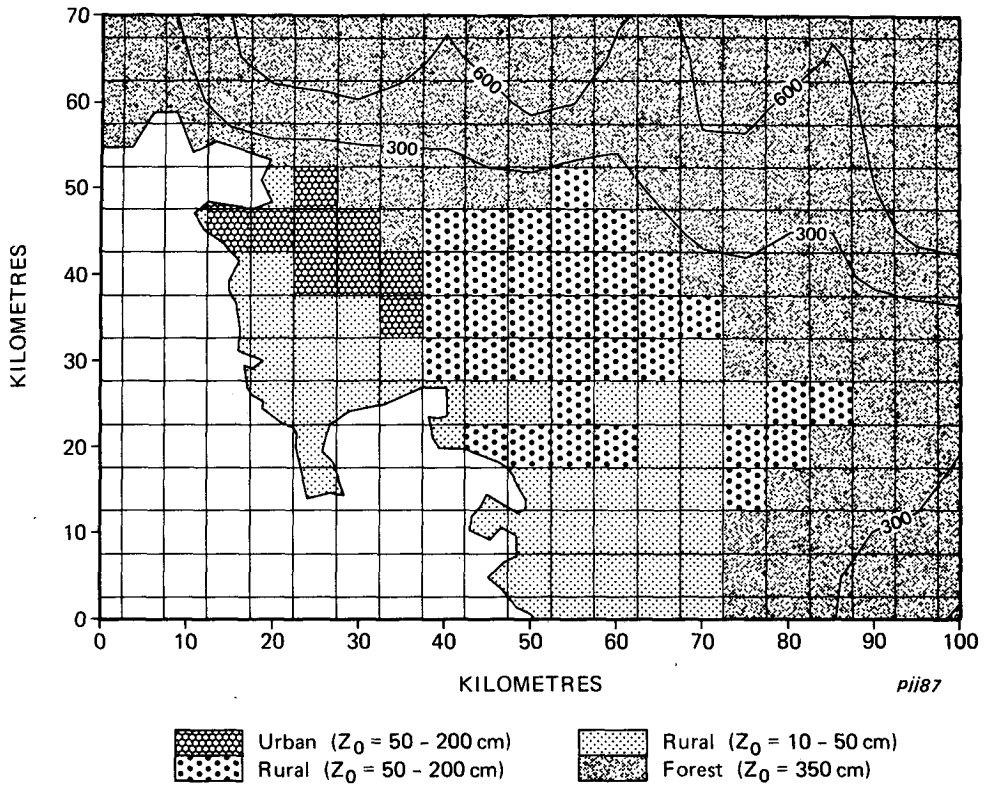

FIG. 2. Map of the modeling domain showing the modeling grid, the land-use types assigned to the grid squares and the smoothed terrain. The shadings refer to the four land-use types defined in Table 1.

poral and spatial resolution of the model. This source of disagreement includes what have been termed subgrid scale effects. In the context of mesoscale modeling of sea breezes, the most important problems are likely to be related to unresolved variations in topographic features and surface properties, and inadequate treatment of convection.

- Inaccuracies in the observed data. While it is conventional to neglect these inaccuracies, it is possible to minimize these problems by locating the sensors away from unresolved topographic features and variations in surface properties. This was attempted in the present study.

It must be presumed that all of the listed sources of disagreement between model and observations exist in a given model evaluation study.

This study employs the methods of Willmott to evaluate the performance of the Colorado State University (CSU) mesoscale numerical model. The model will be evaluated against an extensive set of observed data covering 24 hours during which a sea-breeze circulation was observed in the lower Fraser Valley of British Columbia, Canada (Fig. 1).

2. The model, modeling domain and input data

The model used in this study is a version of the mesoscale numerical model described by Pielke (1974), Pielke and Mahrer (1975, 1978) and Mahrer and Pielke (1977, 1978). The model, which was designed to study thermally forced, terrain-induced mesoscale phenomena, is hydrostatic and consists of the equations of mo-

TABLE 1. Surface properties assigned to the various land-use categories.

Land-use category	Surface roughness length (m)	Albedo (−)	Soil wetness*	Soil specific heat (kJ kg^{-1} K^{-1})	Soil diffusivity (m^2 s^{-1})	Soil density (kg m^{-3})
Urban	0.80	.15	.15	1.20	1.33	1500
Rural	0.20	.23	.30	1.55	0.50	1300
Rural	0.50	.19	.30	1.55	0.50	1300
Forest	3.50	.15	.15	1.21	0.30	1500

* A parameter in the range 0.0 to 1.0 for dry to wet.

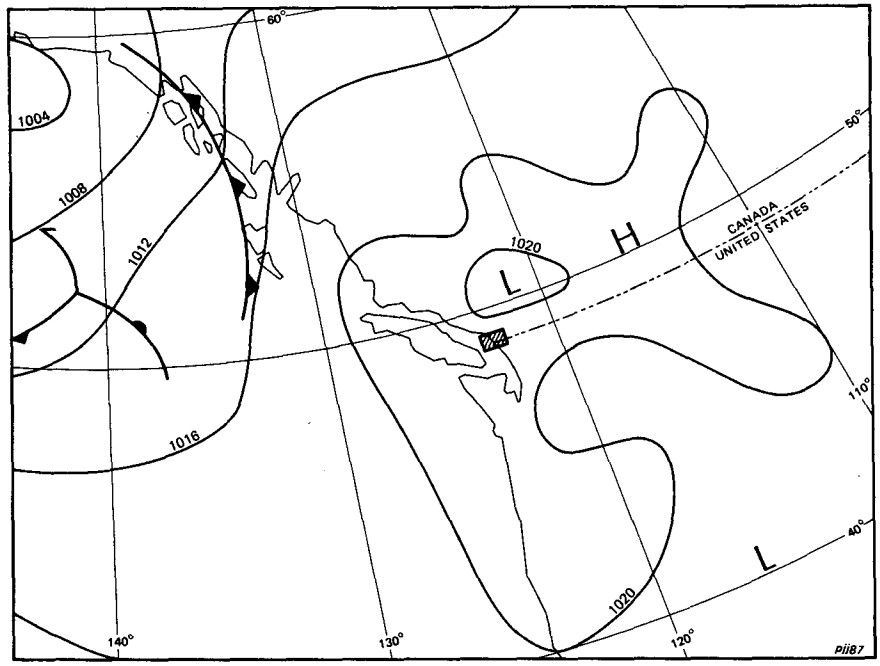

FIG. 3. Synoptic sea-level pressure map of the Northeastern Pacific Ocean valid for 1800 UTC (1000 PST), 23 August 1985. The small square near the center marks the modeling domain.

tion, moisture and continuity within a three-dimensional terrain-following coordinate system. It includes a thermodynamic equation, a diagnostic equation for pressure, a surface heat budget and boundary layer parameterization after Deardorff (1974).

The model version allows for the inclusion of synoptic scale subsidence in the prognostic equation for planetary boundary layer growth since this is known to be significant in the Vancouver region during summer (Steyn 1981). The subsidence (based on a constant synoptic scale horizontal divergence of 0.00007 s^{-1}) represents a summertime average value for the modeled region. The model allowed the inclusion of variable surface properties to more realistically represent the principal land-use variations over the region. The method used was similar to that of Hjelmfelt (1982) and allowed the specification of albedo, soil thermal diffusivity, soil density, soil specific heat, and soil wetness at each grid point. Surface properties were assigned by defining four broad land-use categories representing the urban environment, the forested montane region and two rural types which may be distinguished on the basis of roughness length and albedo (Fig. 2). As there

TABLE 2. Initial vertical profile of potential temperature and specific humidity.

Level	z (m)	Θ (K)	q (−)
1	10	290.2	.0079
2	40	287.0	.0080
3	100	288.4	.0080
4	200	290.2	.0081
5	350	291.8	.0079
6	500	292.5	.0077
7	750	293.6	.0072
8	1000	296.0	.0061
9	1250	299.3	.0045
10	1500	300.0	.0042
11	1750	302.1	.0041
12	2000	303.4	.0039
13	2500	307.6	.0037
14	3000	310.2	.0035
15	3500	311.9	.0033
16	4000	314.0	.0031
17	4500	316.4	.0028
18	5000	318.2	.0025
19	5500	320.0	.0022
20	6000	323.0	.0014
21	6500	324.5	.0010
22	7000	326.0	.0008
23	7500	327.5	.0005
24	8000	329.0	.0003
25	8500	331.5	.0002
26	9000	333.0	.0001

TABLE 3. Input parameters.

Timestep	60 s
Mean latitude	49.0°N
PBL height	150 m
Surface pressure	1021 mb
Sea surface temperature	17.0°C
Free atmospheric lapse rate of potential temperature	6 K km^{-1}
Geostrophic wind	3 m s^{-1} from 040 deg (True)

TABLE 4. Wind field evaluation statistics.

Hour (PST)	n –	RMSD (m s^{-1})	RMSD$_s$ (m s^{-1})	RMSD$_u$ (m s^{-1})	d –	σ_m (m s^{-1})	σ_o (m s^{-1})	$\bar{U}_m$ (m s^{-1})	$\bar{U}_o$ (m s^{-1})	$\bar{\Theta}_m$ (deg)	$\bar{\Theta}_o$ (deg)
0100	19	1.41	1.13	0.84	0.45	0.87	0.71	1.47	0.51	91.5	99.9
0200	19	1.28	1.18	0.48	0.48	0.51	0.78	1.30	0.69	36.2	82.1
0300	19	1.14	1.03	0.51	0.50	0.54	0.79	0.77	0.56	20.0	89.6
0400	19	1.10	0.95	0.54	0.42	0.56	0.59	0.81	0.22	2.6	72.6
0500	19	1.19	1.06	0.55	0.41	0.57	0.65	0.90	0.18	2.6	62.5
0600	19	1.02	0.84	0.58	0.47	0.60	0.79	0.80	0.39	11.3	27.1
0700	19	0.87	0.59	0.63	0.56	0.67	0.70	0.51	0.25	358.0	13.0
0800	19	1.37	1.20	0.66	0.48	0.70	1.23	0.48	0.12	309.0	212.0
0900	24	1.36	1.00	0.92	0.51	0.94	1.12	0.63	0.83	270.0	264.0
1000	24	1.87	1.53	1.07	0.54	1.12	1.45	0.98	1.91	269.0	266.0
1100	24	1.88	1.40	1.26	0.56	1.34	1.55	1.52	2.12	273.0	273.0
1200	24	1.82	1.11	1.43	0.60	1.55	1.53	2.11	2.13	275.0	275.0
1300	24	2.12	1.41	1.57	0.52	1.68	1.56	2.62	2.09	277.0	267.0
1400	24	2.28	1.46	1.75	0.50	1.85	1.62	3.08	2.64	278.0	271.0
1500	24	2.47	1.58	1.90	0.53	1.99	1.88	3.41	2.93	277.0	274.0
1600	24	2.47	1.58	1.91	0.60	2.06	1.94	3.60	2.65	276.0	273.0
1700	23	2.34	1.38	1.89	0.57	2.08	1.53	3.70	2.62	276.0	269.0
1800	23	2.23	1.31	1.81	0.54	1.97	1.25	3.47	2.35	274.0	271.0
1900	23	2.07	1.33	1.59	0.59	1.83	1.18	2.95	1.67	275.0	273.0
2000	24	2.25	1.48	1.70	0.44	1.77	1.13	2.15	0.89	282.0	277.0
2100	24	2.28	1.35	1.84	0.43	1.91	1.08	1.45	0.36	302.0	283.0
2200	24	2.14	0.78	1.99	0.42	2.08	0.81	0.80	0.22	334.0	290.0
2300	24	1.81	0.56	1.72	0.59	1.97	1.01	0.56	0.29	34.7	336.0
2400	23	1.67	1.17	1.19	0.61	1.42	1.07	1.00	0.26	80.4	333.0

Note: 1) The first four rows refer to the period of dynamic initialization explained in section 2. 2) The statistics are all given as averages for the hour ending on the time indicated. 3) All times are Pacific Standard Time which on the day in question (23 August 1985) was 16 minutes ahead of Local Apparent Time. 4) The subscripts o and m indicate observed and modeled values respectively. The columns headed U and Θ contain averages of wind speed and direction over all points i.

is considerable uncertainty regarding the exact spatial and temporal variations in the six surface parameters over the region, values had to be assigned on the basis of a consensus of local experts. These values are considered to be representative of the summer season in the modeled region (Table 1).

The terrain of the modeling domain is shown in Fig. 1. This terrain was averaged upward to 5 km resolution from a 1 km resolution digital terrain dataset (derived from the geomagnetic anomaly files maintained by Energy, Mines and Resources: Canada) and smoothed to remove 2 grid-length variability by application of a 1-2-1 binomial filter.

Data from 23 August 1985 were used to provide initial conditions for the simulation. This day was characterized by clear skies and light winds aloft associated with a broad high pressure region over the British Columbia–Washington coastal zone (Fig. 3), a situation well suited to the unhindered development of thermally driven mesoscale phenomena. The vertical profiles of temperature and humidity (Table 2) used to initialize the model were derived from a composite of the 0545 Pacific Standard Time (PST) tethersonde sounding (to 1.0 km) from within the city of Vancouver and the nearest rawinsonde sounding at Quillayute (200 km to the southwest) taken at 0400 PST. The geostrophic wind (from the Quillayute sounding) was set to 3 m s^{-1} from the northeast and was representative of flow up to approximately 4.0 km. No vertical shear was included above the planetary boundary layer.

The simulation was performed on a 35 × 29 × 26 grid with a horizontal grid spacing of 5 km, except at the six outermost grid points where it expands linearly to 35 km (only the inner 5 km grid (Fig. 2) is represented in subsequent figures). Vertical grid spacing was variable with greatest resolution near the surface (Table 2). An absorbing layer was included above level 17 to control the reflection of vertically propagating wave energy (Klemp and Lilly 1978; Mahrer and Pielke 1978).

Input parameters are presented in Table 3. The simulation commenced at sunrise (0511 PST) and was preceded by a 4-hour period of dynamic initialization in which surface cooling was permitted to occur. This procedure enabled nocturnal flow features to be represented at sunrise and thereby provide a more realistic initial state. The initial temperature profiles for this initialization were adjusted to ensure that after dynamic initialization, the modeled profile matched the sunrise tethersonde profile at the appropriate grid point.

3. Evaluation data

The evaluation was based on data collected by the Greater Vancouver Regional District, the Atmospheric Environment Service, the British Columbia Ministry

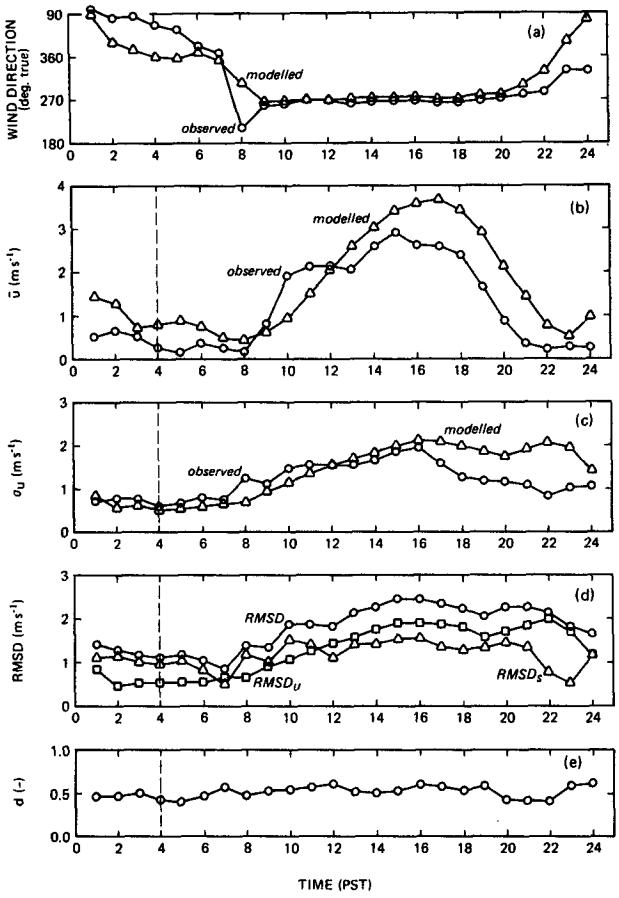

FIG. 4. The evolution of modeled and observed (a) average wind direction, (b) average wind speed, (c) standard deviation of wind speed, (d) total (RMSD), systematic (RMSD$_s$) and unsystematic (RMSD$_u$) root mean square deviations and e) index of agreement for 23 August 1985.

of Environment and the University of British Columbia Geography Department (UBC). The observation network used for this evaluation is displayed in Fig. 1.

Surface wind speed and direction (10 m) were monitored continuously at 24 locations across the domain. The nine UBC stations were sited to augment the existing 15 stations for the purpose of this study. This resulted in a network with a mean nearest neighbor distance of 7.3 km and standard deviation of 4.5 km.

Identical shielded thermistors were installed at 10 m AGL at eight of the UBC anemometer sites to provide data for comparison with modeled air temperatures. In addition, the energy balance components Q^* (surface net all-wave radiative flux density) and Q_H (sensible turbulent heat flux density) were available from direct measurements until midafternoon from a suburban location. The ground heat flux Q_G was calculated using a parameterization developed by Oke et al. (1981) while Q_E (the latent turbulent heat flux density) was calculated by residual.

Vertical variations in wind speed and direction, temperature and humidity were derived from tethersonde soundings at a single urban site during daylight hours. Soundings were made continuously and took approximately one hour for an ascent and descent. Three acoustic sounders located in the Lower Fraser Valley were also used to monitor vertical thermal structure and to give an indication of mixed layer depth.

4. Results and evaluation

The evaluations are performed by comparison between hourly averages of modeled and observed wind velocities and temperatures. In general, the points at which the data are measured do not correspond with points on the model grid. To overcome this difficulty, modeled output values from the four grid points nearest to the measurement point are interpolated (with inverse square distance weighting) to provide modeled values at the measurement points.

a. Wind fields

Figure 1 shows that the observational network measures winds in the valley, but not on the valley walls. While the model and its input data do reflect the real topography, the degree of smoothing required to suppress numerical artifacts dictates that this modeling exercise (based on a 5 km grid) will only resolve flow features forced by the gross valley dimensions. A smaller grid spacing is not permitted because the steep slopes of the valley walls, if more precisely resolved, would violate the hydrostatic assumption inherent in the model formulation. The present grid spacing was chosen as a safe lower limit, with somewhat higher resolution than the measured data. The following discussion of the evaluation statistics in Table 4 will address the model's precision and accuracy in reproducing the observed sea breeze.

Figures 4a–e indicate the evolution of the wind field evaluation statistics displayed in Table 4. From Figs. 4a, 4b it is clear that the overall evolution of the observed and modeled fields are in close agreement. As Fig. 4b indicates, both observed and modeled winds display a maximum in magnitude at roughly 1500 to 1700 PST, with the modeled speeds exceeding those observed by up to 1 m s^{-1} at times. Figure 4c indicates that the modeled field has a spatial standard deviation that closely matches the observed one for all hours except those between 1700 and 2300 PST when the modeled standard deviation is considerably larger than the observed. This is due to the model producing a combination of strong upslope winds in the northeastern portions of the domain and strong northwest winds over the waters of the southwestern portions of the domain in the late afternoon and evening (see Fig. 5b). The presence of these features results in a spatial back-

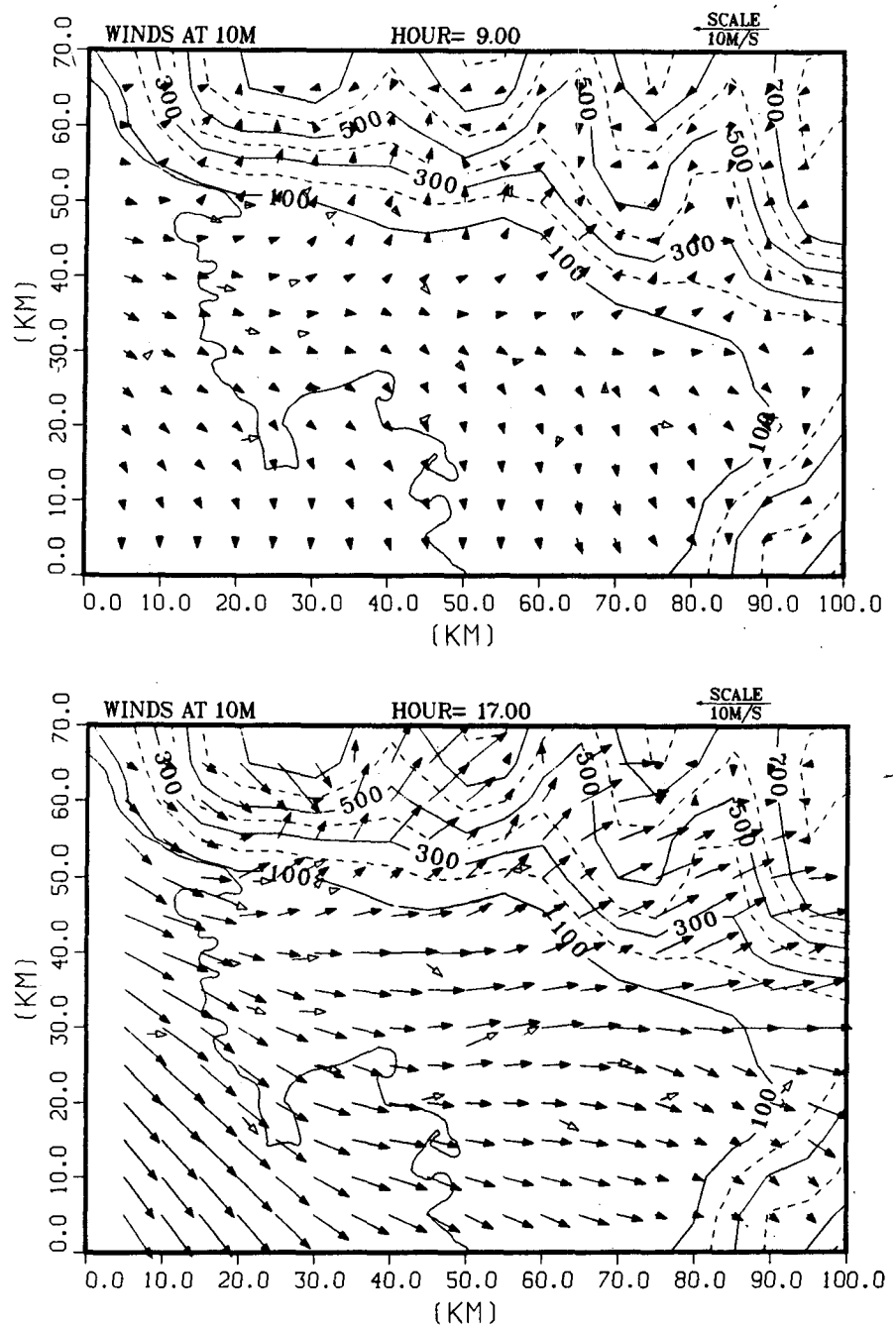

FIG. 5. Observed and modeled wind vectors at 0900 PST and 1700 PST 23 August 1985. The open arrows are the observed winds and the contours are the smoothed terrain.

ing of the wind from the west to east sides of the domain, and results in the relatively large modeled standard deviations in the later part of the day. The observing network did not extend into the steep northern portions of the domain and therefore cannot completely resolve the upslope winds whose effects are just visible in the northeastern stations. The coastal stations do indicate that the strong winds modeled over the water are present in reality. Figure 4d shows the evolution of the root mean square deviation and its two components. According to the interpretations of Willmott, the unsystematic component represents the irreducible deviation between observed and modeled results, while the systematic component represents trendlike differences between observed and modeled fields. In this case, both components of the RMSD are

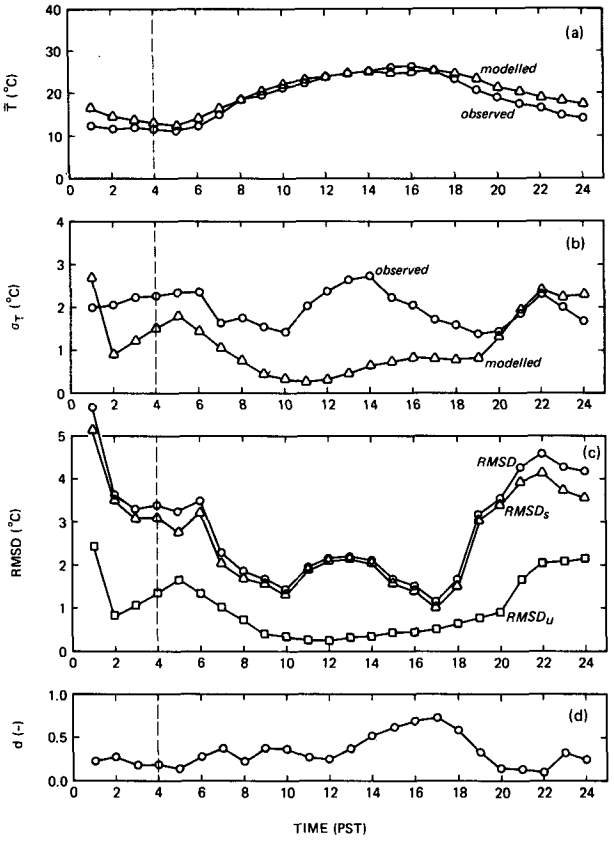

FIG. 6. Evolution of the modeled and observed (a) average temperature, (b) standard deviation of temperature, (c) total (RMSD), systematic (RMSD$_s$) and unsystematic (RMSD$_u$) root-mean-square deviations of temperature, and (d) index of agreement for 23 August 1985.

of roughly equal magnitude, and vary in unison with the mean wind. It must be presumed that the systematic component is largely due to the spatial backing already referred to since this backing is more evident in the modeled than observed fields.

As shown on Figure 4e, the index of agreement (d) varies between 0.41 and 0.61 with no systematic trends. The absence of trends in d indicates that the model is capable of reproducing the general evolution of the sea breeze. This index of agreement is most useful in making cross-comparisons between models (Willmott 1982) a task beyond the scope of this paper.

The model's performance is further illustrated by examining Figs. 5a and 5b, which are plots of modeled and observed wind vectors at 0900 and 1700 PST. At 0900 PST the modeled winds in the land covered portions of the domain show distinct but still weak landward and/or upslope components, with magnitudes and directions generally in agreement with the observed ones. The plot for the hour ending 1700 PST covers the time of peak intensity of the modeled sea breeze. This plot gives a visual impression of the excess modeled (when compared with observed) wind speeds at this time, and illustrates the spatial backing alluded to earlier.

b. *Temperature fields*

The temperature fields are evaluated using a network of eight thermometers located in the central part of the Fraser Valley as indicated in Fig. 1.

Figures 6a–d show the evolution of the evaluation statistics displayed in Table 5. From Fig. 6a it is clear

TABLE 5. Temperature field evaluation statistics.

Hour	n –	RMSD (°C)	RMSD$_s$ (°C)	RMSD$_u$ (°C)	d –	σ_m (°C)	σ_o (°C)	$\bar{T}_m$ (°C)	$\bar{T}_o$ (°C)
0100	8	5.68	5.14	2.43	0.21	2.71	2.00	16.6	12.2
0200	8	3.66	3.57	0.82	0.28	0.91	2.07	14.6	11.8
0300	8	3.31	3.14	1.06	0.19	1.21	2.23	13.9	12.0
0400	8	3.40	3.11	1.37	0.19	1.51	2.26	13.1	11.2
0500	8	3.26	2.80	1.67	0.15	1.80	2.35	12.4	11.0
0600	8	3.50	3.23	1.35	0.28	1.48	2.39	14.1	12.2
0700	8	2.29	2.06	1.01	0.38	1.09	1.63	16.4	15.2
0800	8	1.86	1.71	0.73	0.23	0.78	1.75	18.4	18.6
0900	8	1.65	1.60	0.40	0.39	0.43	1.55	20.4	19.6
1000	8	1.41	1.38	0.32	0.38	0.34	1.42	21.8	21.3
1100	8	1.92	1.90	0.25	0.28	0.27	2.04	22.9	22.6
1200	8	2.12	2.10	0.26	0.26	0.31	2.38	23.8	23.8
1300	8	2.19	2.17	0.31	0.38	0.46	2.64	24.6	24.6
1400	8	2.10	2.07	0.35	0.52	0.63	2.71	25.0	25.1
1500	8	1.65	1.60	0.43	0.63	0.76	2.24	25.3	25.7
1600	8	1.50	1.44	0.43	0.69	0.83	2.08	25.3	26.0
1700	8	1.13	1.02	0.50	0.74	0.81	1.70	25.2	25.2
1800	8	1.66	1.52	0.65	0.59	0.79	1.57	24.6	23.6
1900	8	3.16	3.07	0.77	0.34	0.85	1.38	23.2	20.5
2000	8	3.52	3.40	0.89	0.15	1.32	1.43	21.4	18.8
2100	8	4.25	3.91	1.65	0.14	1.97	1.85	20.1	17.1
2200	8	4.59	4.12	2.03	0.11	2.39	2.33	18.9	16.3
2300	8	4.26	3.72	2.09	0.34	2.23	2.00	18.1	14.8
2400	8	4.16	3.55	2.16	0.25	2.32	1.64	17.2	14.0

Note: 1) Notes 1 to 4 on Table 4 also apply to this table. 2) The columns headed T contain averages of temperature over all points i.

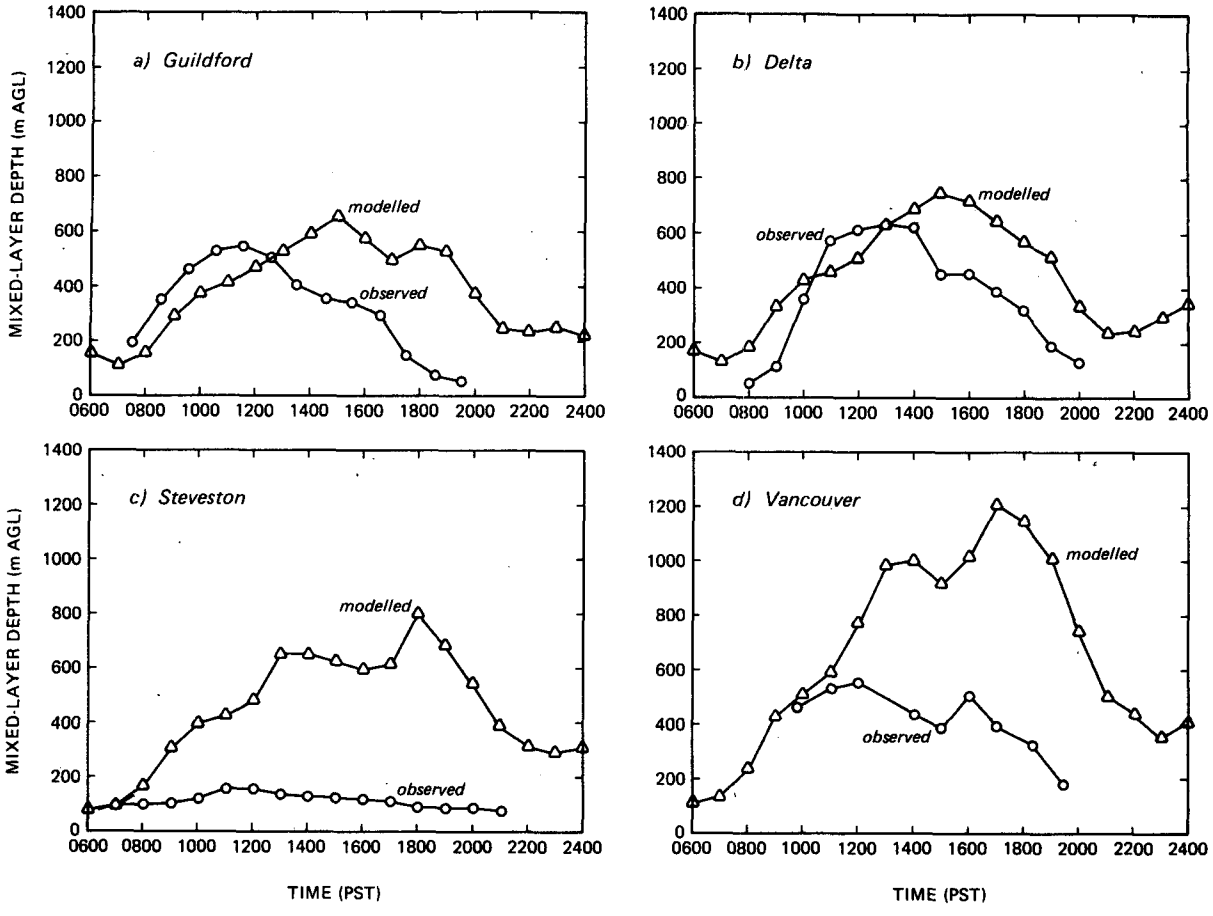

FIG. 7. Evolution of the modeled and observed mixed layer depth at the (a) Guildford, (b) Delta, (c) Steveston and (d) Vancouver stations. (See Fig. 1 for the station locations.)

that the modeled and observed mean temperatures are in close agreement, while Fig. 6b shows that there is considerably more spatial variance in the observed field than in the modeled. This is presumably due to local (subgrid scale) variations in surface properties that affect the surface energy budgets and hence the near-surface temperature. As noted in section 2, the spatial resolution of surface properties provided as model input is considerably less than the grid spacing. It should therefore not be surprising that the low-level modeled temperature field has less structure than that observed. The dominance of the systematic RMSD (Fig. 6c) is due to smaller than observed variance in the modeled temperature field while the two means are in agreement. This results in the observed versus modeled regression having a slope different than unity, and hence a large systematic RMSD. The fact that the mean air temperatures are in good agreement is an indication that the energy totals are properly distributed between the energy budget terms (particularly that the sensible heat flux is well modeled), and that the advection and diffusion of heat within the model are sufficiently strong. Of relevance is the better performance of the model during daylight hours when higher temperatures and wind speeds reflect the generally unstable conditions which are better modeled by the Monin-Obukhov similarity scheme than are the stable conditions found at night. The index of agreement (d) is generally low (0.20 to 0.35) throughout the morning and night, and rises to a maximum of 0.75 at the time of peak sea breeze intensity.

c. *Surface energy fluxes*

The model being examined is particularly suited to the study of mesoscale atmospheric phenomena that are thermally forced. Because of this, it is important to ensure that the model faithfully reflects the partition of solar and thermal radiation at the Earth's surface into sensible, latent and subsurface conducted components. Figures 8a–c show the evolution of these three fluxes at one point in the modeling domain.

In Fig. 8a the modeled values are compared with directly measured values of the turbulent sensible heat flux. The measurements were made for the hours ending 0600 to 1500 PST using eddy correlation instrumentation on the tower in the suburban location de-

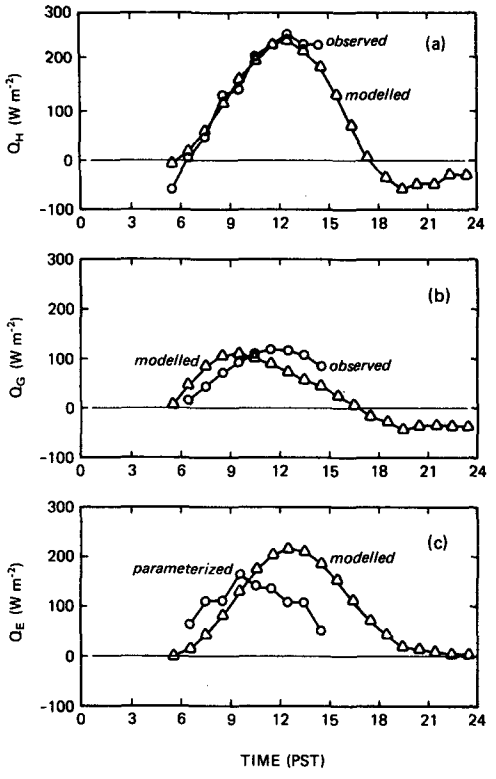

FIG. 8. The evolution of modeled and observed (a) turbulent sensible heat flux, (b) subsurface conductive heat flux, and (c) turbulent latent heat flux at the Vancouver station. (See Fig. 1 for the station location.)

scribed by Cleugh and Oke (1986). There is very close agreement between modeled and observed fluxes.

In Fig. 8b the modeled conductive flux is compared with the flux derived from the parameterization given by Oke et al. (1981). The fluxes are in general agreement, with the modeled fluxes leading the parameterized ones by two to three hours.

The turbulent latent heat fluxes are compared in Fig. 8c. In this diagram, the observed fluxes are derived by subtracting the above sensible and conductive fluxes from the measured net all wave radiation. The modeled and observed fluxes have a similar magnitude, but are out of phase by roughly three hours with the modeled flux lagging the observed.

d. *Mixed layer depth*

Data on the boundary layer depth were available at four points in the modeling domain, as indicated in Fig. 1. At three of those points, acoustic sounders provided continuous traces of the height of the inversion capping the mixed layer, while profiles of temperature from a tethersonde operated at the fourth point gave the same data at nine times during the day. These data are plotted on Figs. 7a–d, together with the modeled values. The modeled mixed layer depths are given as instantaneous values each hour, and were interpolated using inverse square distance weighting from the four grid points nearest the point of observation.

Figures 7a and 7b indicate that the modeled mixed layer depths at Guildford and Delta correspond reasonably well with the observed ones in the early part of the day, but diverge somewhat in the afternoon when the modeled depths remain elevated while the observations show the mixed layer to be decreasing in depth. The observed mixed layer evolution at both sites is consistent with the results of Steyn and Oke (1982) who studied the effects of advection on the mixed layer depth in this region.

Figure 7c indicates that the model overestimates the very shallow mixed layer depth observed at this coastal location where advection of cool marine air is effective in suppressing its rise. This is to be expected, since the model contains horizontal numerical smoothing, which will tend to suppress the effects of the land–sea discontinuity in its immediate vicinity.

Figure 7d indicates that the modeled mixed layer depth at the Vancouver station rises throughout the day to a maximum of 1200 m above ground level at 1700 PST and drops sharply thereafter, while the observed depth reaches its maximum of 560 m at noon and falls rather slowly through the afternoon. While a detailed examination of this question is beyond the scope of this paper, an examination of the relevant model variables suggests that the computed vertical velocity field near the steep terrain in the north of the model domain is the cause of this disagreement.

e. *Profiles*

While the model under consideration is fully three-dimensional, the evaluation data used in sections 4a–c are for near-surface values of the model variables. For many applications however, wind fields well above the surface layer are required. For this reason we present a test of the model's ability to simulate wind profiles at one point in the domain.

Vertical profiles of the east–west and north–south velocity components as observed and modeled at Vancouver are plotted for the hours 0900, 1200, 1500 and 1800 in Figs. 9a–d and 10a–d. The observed data show a strong bias toward flow along the east–west axis throughout the day with predominantly westerly (onshore) flow in the layer up to 500 m and east to southeasterly flow aloft. The modeled profiles after 1200 PST show a layer of onshore wind considerably deeper and with higher wind speeds within that layer than observed. By contrast, Fig. 9a indicates that at 0900 PST, the modeled layer of onshore wind is shallower and of lower intensity than observed.

Consideration of the north–south velocity component (Fig. 10) indicates that the modeled winds have a greater northerly component in the upper layers of the domain than observed. This is most obvious at

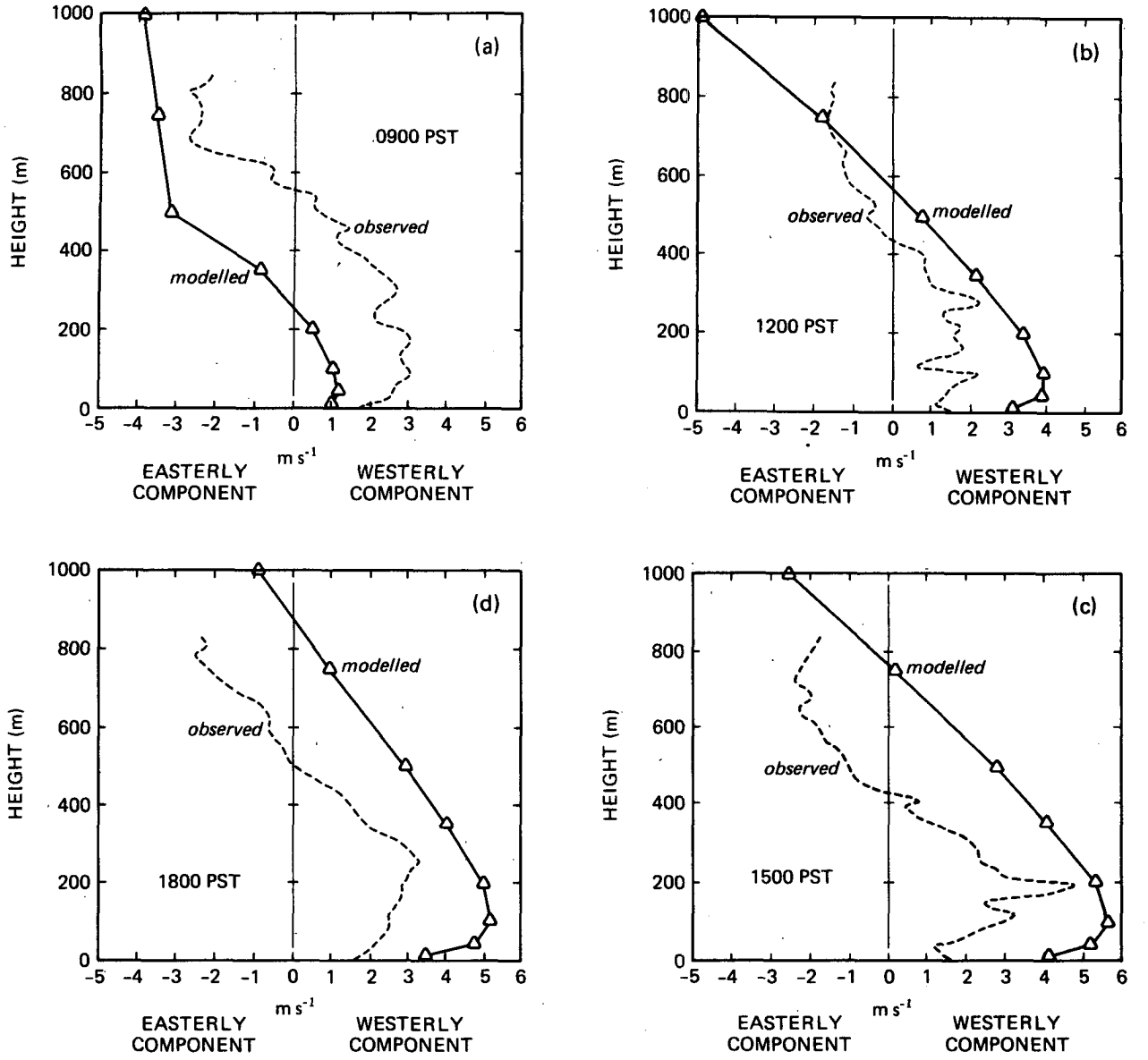

FIG. 9. Profiles of the east–west component of wind velocity at (a) 0900 PST, (b) 1200 PST, (c)1500 PST, and (d) 1800 PST as measured at Vancouver and modeled. The dashed line is the measured profile.

upper-levels and may be attributed to the rather inexact specification of the initial wind profile used in the model. It is also likely that the process of terrain smoothing would contribute to a lack of agreement between the observed and modeled three-dimensional wind field in the lee of the terrain in the northern section of the model domain.

5. Conclusions

The quantitative model evaluation statistics used have shown that in general, the model performs well in simulating both spatial and temporal variability of a sea breeze in the chosen domain. The graphic representation of the wind fields forms a useful adjunct to these statistics and is invaluable in identifying areas of particular disagreement that are lost in the statistics.

While the general features of the phenomenon are well modeled, the model performs less well during the night, and has some difficulty with the afternoon transition between land- and sea-breeze regimes. The model has a tendency to overestimate wind speed during the daytime. The modeled mixed-layer depths match closely the observed ones in the morning, but remain elevated through the afternoon when the observations indicate slowly reducing mixed layer depths. The model

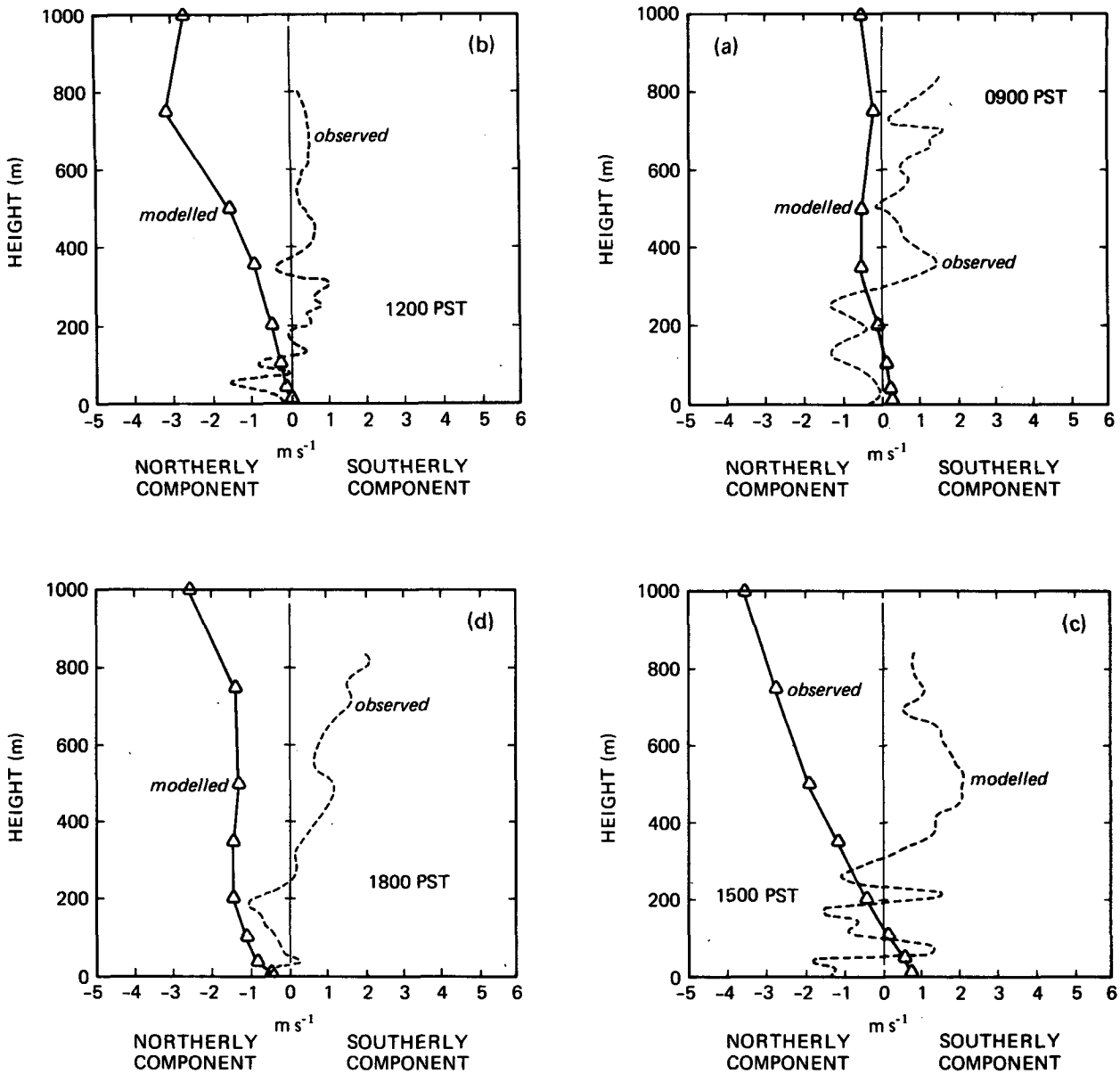

FIG. 10. As in Fig. 9 but of the north–south component of wind velocity.

indicates greater than observed mixed layer depths in the nearshore zone where advection is effective in limiting them. It is shown that the shapes of the east–west wind profiles are similar to the observed ones, with the model having a tendency to overestimate the strength of onshore winds. The modeled and observed surface fluxes are shown to be in close agreement, as are the near surface temperatures.

The model has performed well in simulating sea breezes in the lower Fraser Valley, B.C., on one day. While this result (being derived from a single case study) cannot serve to justify its use without question, it does indicate the degree of veracity of the particular model.

Acknowledgments. Funding support for this work was provided by grants from The Natural Science and Engineering Research Council of Canada, contracts from the British Columbia Ministry of Environment and Science Subventions from Environment Canada. Dr. Roger Pielke kindly provided the model while Dr. Ray Arritt was extremely helpful in guiding us in the model implementation, and in overcoming runtime errors. Drs Richard Bennett and Mike Novak and Mr. Kirk Johnstone provided valuable data on soil properties in the lower Fraser Valley. While many assistants helped in gathering the evaluation data, the efforts of Keith Ayotte and Helen Cleugh are particularly ap-

preciated. Dr. Tim Oke and two anonymous reviewers provided valuable comments on early versions of the manuscript. Paul Jance drafted the diagrams.

REFERENCES

Cleugh, H. A., and T. R. Oke, 1986: Suburban–rural energy balance comparisons in the summer for Vancouver, B.C. *Bound.-Layer Meteor.*, **36**, 351–369.

Deardorff, J. W., 1974: Three dimensional numerical study of the height and mean structure of a heated planetary boundary layer. *Bound.-Layer Meteor.*, **7**, 81–106.

Hjelmfelt, M. R., 1982: Numerical simulation of the effects of St. Louis on mesoscale boundary layer airflow and vertical air motion: simulations of urban vs non-urban effects. *J. Appl. Meteor.*, **21**(9), 1239–1257.

Keyser, D., and R. A. Anthes, 1977: The applicability of a mixed-layer model of the planetary boundary layer to real data forecasting. *Mon. Wea. Rev.*, **105**, 1351–1370.

Klemp, J. B., and D. K. Lilly, 1978: Numerical simulation of hydrostatic mountain waves. *J. Atmos. Sci.*, **32**, 78–107.

Mahrer, Y., and R. A. Pielke, 1977: The effects of topography on sea and land breezes in a two dimensional numerical model. *Mon. Wea. Rev.*, **105**, 1151–1162.

——, and ——, 1978: A test of an upstream spline interpolation technique for the advection terms in a numerical mesoscale model. *Mon. Wea. Rev.*, **106**, 818–830.

Oke, T. R., B. D. Kalanda and D. G. Steyn, 1981: Parameterization of heat storage in urban areas. *Urban Ecol.*, **5**, 45–54.

Pielke, R. A., 1974: A three dimensional numerical model of the sea breeze over south Florida. *Mon. Wea. Rev.*, **102**, 115–134.

——, 1984: *Mesoscale Meteorological Modeling.* Academic Press, 612 pp.

——, and Y. Mahrer, 1975: Representation of the heated planetary boundary layer in mesoscale models with coarse vertical resolution. *J. Atmos. Sci.*, **32**, 2288–2308.

——, and ——, 1978: Verification analysis of the University of Virginia three-dimensional mesoscale model prediction over south Florida for 1 July 1973. *Mon. Wea. Rev.*, **106**, 1568–1589.

Segal, M., Y. Mahrer and R. A. Pielke, 1982: Application of a numerical mesoscale model for the evaluation of seasonal persistent regional climatological patterns. *J. Appl. Meteor.*, **21**, 1754–1762.

Simpson, J., N. E. Westcott, R. J. Clerman and R. A. Pielke, 1979: On cumulus mergers. *Arch. Met. Geophys. Bioklim.*, **A29**, 1–40.

Steyn, D. G., 1981: *Turbulence, Diffusion, and the Daytime Mixed Layer Depth over a Coastal City*, Unpublished Ph.D. thesis, The University of British Columbia, Vancouver, Canada, V6T 1W5, 161 pp.

——, and T. R. Oke, 1982: The depth of the daytime mixed layer at two coastal locations: A model and its validation. *Bound.-Layer Meteor.*, **24**, 161–180.

Willmott, C. J., 1981: On the validation of models. *Phys. Geogr.*, **2**, (2), 168–194.

——, 1982: Some comments on the evaluation of model performance. *Bull. Amer. Meteor. Soc.*, **63**(11), 1309–1313.

——, S. G. Ackleston, R. E. Davis, J. J. Feddema, K. M. Klink, D. R. Legates, J. O'Donnell and C. M. Rowe, 1985: Statistics for the evaluation and comparison of models. *J. Geophys. Res.*, **90**(C5), 8995–9005.